High-Pressure Structures and Transformations of Calcium Borohydride Probed by Combined Raman and Infrared Spectroscopies

Ang Liu, Shuntai Xie, Shahab Dabiran-Zohoory, and Yang Song*

Department of Chemistry, The University of Western Ontario, London, Ontario N6A 5B7, Canada

Received: January 31, 2010; Revised Manuscript Received: May 29, 2010

Calcium borohydride ($Ca(BH_4)_2$) has attracted significant interest in recent years due to its strong potential for hydrogen storage applications. Here, we report the pressure-induced structural transformations of $Ca(BH_4)_2$ probed by combined Raman spectroscopy and infrared (IR) spectroscopy up to 10.4 GPa at room temperature. Starting with the α phase in an orthorhombic structure, $Ca(BH_4)_2$ was found to undergo several transformations upon compression, as evidenced by the sequential changes of characteristic Raman and IR modes as well as by examining the pressure dependences of these modes. In situ Raman and IR measurements collectively provided consistent information about the structural evolutions of $Ca(BH_4)_2$ under compression. Decompression measurements on $Ca(BH_4)_2$ suggest that the pressure-induced transformations are reversible in the entire pressure region. The combined Raman and IR data allowed for an in-depth analysis of possible high-pressure structures of $Ca(BH_4)_2$.

Introduction

Recently, calcium borohydride ($Ca(BH_4)_2$) has been the focus of extensive studies because of its strong potential for hydrogen storage applications.[1−14] With a gravimetric hydrogen density of 11.5 wt %, $Ca(BH_4)_2$ exhibited a reversible or at least a partially reversible (de)hydrogenation ability under high-temperature/pressure conditions via different reaction pathways, such as illustrated in the following.[1,8,12]

$$Ca(BH_4)_2 \rightarrow CaH_2 + 2B + 3H_2 \quad (1)$$

$$3Ca(BH_4)_2 \rightarrow 2CaH_2 + CaB_6 + 10H_2 \quad (2)$$

At a pressure of 9 MPa, Kim et al.[8] reported that hydrogen can be reversibly produced via reaction 1, thus yielding a hydrogen capacity of 8.7 wt %. Subsequently, Ronnebro et al.[12] reported an even higher reversible capacity of 9.6 wt % via reaction 2 at 620−660 K and 700 bar. More recently, Wang et al.[1] conducted both experimental and theoretical studies on the reversibility of the above reactions and proposed a reaction intermediate in the form of $Ca(B_{12}H_{12})$, an energetically favorable structure that possibly plays an important role in the (de)hydrogenation process.

Depending on the detailed synthetic conditions, different crystal structures were observed for $Ca(BH_4)_2$ as characterized by X-ray diffraction, neutron diffraction, and vibrational spectroscopy as well as by theoretical investigations.[2,3,5,6,9,10,13,14] For instance, $Ca(BH_4)_2$ prepared by desolvation of the commercial $Ca(BH_4)_2 \cdot 2THF$ at 433K for 1 h crystallizes into the α phase with an orthorhombic structure (shown in Figure 1a),[14] which is believed to be the primary stable phase at both room and lower temperatures. However, other space groups were also proposed later,[2,5] making the structure of the α-phase $Ca(BH_4)_2$ still controversial. Upon annealing to high temperature[9] or by ball-milling,[2] α-phase $Ca(BH_4)_2$ can be irreversibly transformed to a new structure (labeled as β phase, Figure 1b). Alternatively, β-phase $Ca(BD_4)_2$ can be directly synthesized by a solid−gas reaction among MgB_2, CaD_2, and D_2 under high T−P conditions.[10] Similarly, although believed to have a tetragonal structure, the exact space group for β-phase $Ca(BH_4)_2$ is also

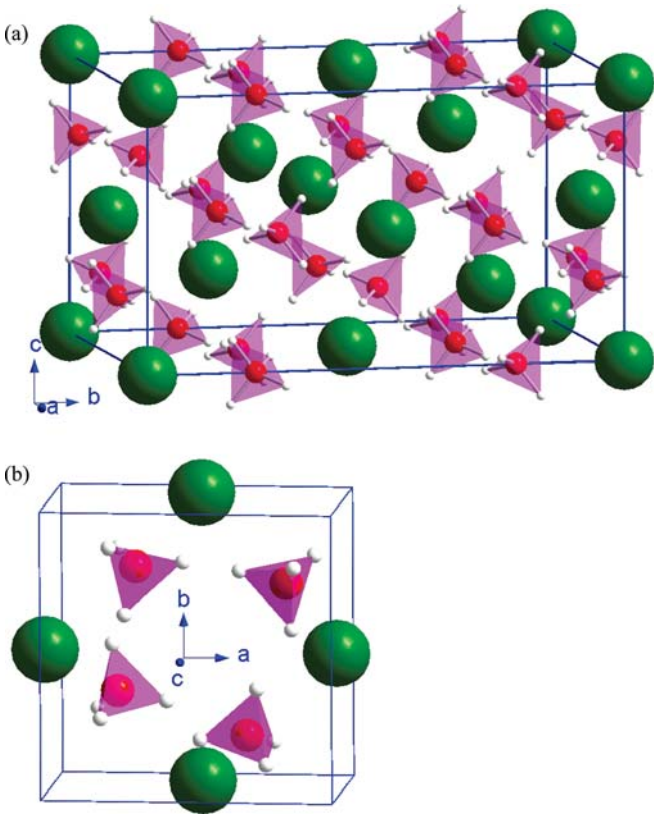

Figure 1. Crystal structures of α-$Ca(BH_4)_2$ in space group *Fddd* (a) and β-$Ca(BH_4)_2$ in space group $P\bar{4}$ (b). The coordinate systems to show the orientations of the unit cell are indicated. The color codes for atoms are green (calcium), pink (boron), and white (hydrogen). Each BH_4^- unit is shown by a tetrahedron.

* To whom correspondence should be addressed. E-mail: yang.song@uwo.ca. Phone: (519)661-2111, ext 86310. Fax: (519)661-3022.

10.1021/jp1009115
Published on Web 06/16/2010

controversial.[2,5,6] Furthermore, during the heating process of α-$Ca(BH_4)_2$, additional polymorphs (e.g., α′, γ, and σ phases) were also reported.[2,5,6,13]

Despite the extensive studies in different temperature regions, little is known about the structures and properties of $Ca(BH_4)_2$ under high pressures.[15] Recent developments in hydrogen storage materials by high-pressure tuning have demonstrated great promises. For instance, H_2 was found to form stable complexes with methane,[16] clathrate hydrate,[17] and even silane at high pressures.[18] More relevantly, another molecular boron hydride, NH_3BH_3, which is considered to be a promising hydrogen storage agent,[19] was found to form a $NH_3BH_3-H_2$ complex upon compression, thus exhibiting an enhanced hydrogen storage capacity.[20] Therefore, understanding the structures and stabilities as well as the reactivities of $Ca(BH_4)_2$ at high pressures constitutes an important aspect for the further development of $Ca(BH_4)_2$-based hydrogen storage materials. To date, the only high-pressure study of $Ca(BH_4)_2$ was recently reported by George et al.[15]

In this study, we report the high-pressure behaviors of pure α-$Ca(BH_4)_2$ to ∼10 GPa in diamond anvil cells (DACs) probed by combined IR and Raman spectroscopic techniques. To our knowledge, this work represents the first in situ high-pressure IR measurements on $Ca(BH_4)_2$ and is the first high-pressure study of pure α-phase $Ca(BH_4)_2$. Because all the fundamental vibrational frequencies of BH_4^- lie coincidentally in the proximity of the very intense (both the first- and the second-order) Raman modes of diamond, structural characterization using Raman spectroscopy only is difficult and subject to ambiguity. The current study represents a significantly improved experimental work in which high-quality Raman spectroscopic data in both the BH_4^- deformation region and the lattice region that were missing from the previous studies[15] were carefully obtained and analyzed. More importantly, all of the fundamental internal vibrational frequencies were clearly resolved in IR spectroscopy without interference. Detailed spectroscopic analyses based on combined Raman and IR activities of the characteristic modes of $Ca(BH_4)_2$ allowed for a more in-depth understanding of the structures and stabilities of several polymorphs of $Ca(BH_4)_2$ that were previously controversial.

Experimental Section

The starting material was prepared from commercial $Ca(BH_4)_2 \cdot 2THF$ (98%, Aldrich). Adduct-free α-$Ca(BH_4)_2$ was obtained by heating $Ca(BH_4)_2 \cdot 2THF$ at 433 K under vacuum for 1 h to remove THF.[9] The prepared sample was examined by ambient-pressure IR and Raman spectroscopies to confirm the phase identity and purity. A symmetric DAC with type II diamonds with a 400 μm culet was used for the IR experiments, whereas type I diamonds with a 400 μm culet were used for Raman experiments. The sample was loaded into the sample chamber created by drilling a 150 μm wide hole on a 70 μm thick stainless steel gasket. Spectral grade KBr powders were also loaded into the DAC used both as a pressure-transmitting medium and to dilute the sample for IR measurements. To accommodate the hygroscopicity of the material, all loadings were done in a nitrogen-filled glovebox (MBraun LABmaster 130), where both water and oxygen levels were maintained below 10 ppm. The pressure was determined from the R_1 ruby fluorescence line with an accuracy of ±0.05 GPa under quasi-hydrostatic conditions.[21] Due to the high sensitivity of $Ca(BH_4)_2$ to moisture, no fluid pressure-transmitting medium was used. However, ruby fluorescence spectra obtained on different ruby chips across the sample chamber indicate no significant pressure gradient. In the entire pressure region (e.g., 0−10 GPa), the ruby spectral profiles suggest that there were no obvious nonhydrostatic effects.

The Raman spectra were collected using a customized Raman microspectroscopy system. A 514 nm Innova Ar^+ laser from Coherent Inc. was used as the exciting source. The laser was focused to less than 5 μm on the sample with an average power of ∼30 mW by an Olympus objective. The Raman signal was detected with a backscattering geometry by the same objective lens. A pair of notch filters were used to remove the Rayleigh scattering, thus enabling a measurable spectral range above 100 cm^{-1}. The Raman photons were dispersed by an 1800 line/mm grating with a 0.1 cm^{-1} resolution and were collected by an ultrasensitive liquid-nitrogen-cooled, back-illuminated charge-coupled device (CCD) detector from Acton. The system was calibrated by neon lines with an uncertainty of ±1 cm^{-1}.

A customized IR microspectroscopy system was used for all IR absorption measurements, and the detailed instrumentation has been described elsewhere.[22] Briefly, a commercial Fourier transform infrared (FTIR) spectrometer from Bruker Optics Inc. (model Vertex 80v) equipped with a Globar IR light source constituted the main component of the micro-IR system, which was operated under a vacuum of <5 mbar, such that the absorption by H_2O and CO_2 was efficiently removed. A collimated IR beam was focused onto the sample in the DAC by a reflective objective. The size of the IR beam was set to be identical to that of the entire sample size (e.g., ∼150 μm) by using a series of iris apertures. The transmitted IR beam was collected using another identical reflective objective as the condenser and was directed to a midband mercury cadmium telluride (MCT) detector equipped with a ZnSe window that allows a measurable spectral range of 600−12 000 cm^{-1}. All measurements were undertaken in transmission (or absorption) mode with a resolution of 4 cm^{-1}. The reference spectrum, that is, the absorption of diamond anvils loaded with KBr but without any sample, was later divided as background from each sample spectrum to obtain the absorbance.

Results and Discussion

A. Ambient-Pressure Raman and IR Spectra. Raman and IR spectra of the prepared $Ca(BH_4)_2$ were collected under ambient conditions and are depicted in Figure 2. According to the previous studies using vibrational spectroscopy and X-ray diffraction,[9,14] $Ca(BH_4)_2$ prepared by the method described in this study is adduct-free crystalline α phase. As can been seen, both our Raman and IR spectra of α-$Ca(BH_4)_2$ are in excellent agreement with those previously reported, indicating the correct phase identity and high purity of our sample. Under ambient conditions, α-$Ca(BH_4)_2$ crystallizes into an orthorhombic structure with space group *Fddd* (D_{2h}^{24}).[14] In each unit cell, there are eight formula units with Ca^{2+} cations on D_2 sites and BH_4^- anions on C_2 sites (Figure 1). Upon factor group analysis, 66 optical modes are predicted for α-$Ca(BH_4)_2$, out of which 36 modes are associated with internal BH_4^- vibrations with the following irreducible representation

$$\Gamma_{\text{internal vib}}^{BH_4^-} = 5A_g + 4B_{1g} + 5B_{2g} + 4B_{3g} + 5A_u + 4B_{1u} + 5B_{2u} + 4B_{3u} \quad (3)$$

where all gerade modes are Raman-active and ungerade modes are IR-active, except for A_u, which is neither Raman- nor IR-active. These 36 internal modes can be considered to originate from the vibrations of a free BH_4^- ion due to a static field

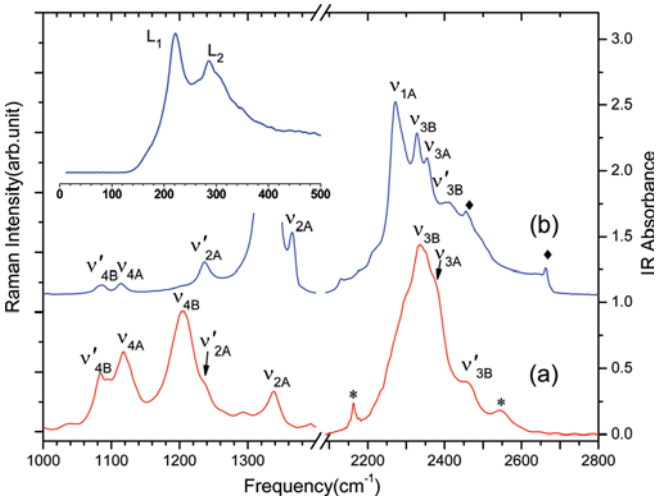

Figure 2. IR absorbance spectrum of $Ca(BH_4)_2$ (a) in comparison with the Raman spectrum (b) in the spectral region of 1000−2800 cm^{-1}, both collected at near ambient pressure and room temperature. The left vertical axis indicates the normalized Raman intensity in arbitrary units, whereas the right vertical axis denotes the absolute IR absorbance intensity. Due to the intense T_{2g} Raman mode of diamond anvil at 1332 cm^{-1}, and the lack of vibrational features in the region of 1400−2100 cm^{-1}, those regions are truncated. The assignments of each Raman IR mode are labeled above the spectra following the conventions discussed in the text. The asterisks above the IR spectrum denote overtones or combinations of fundamentals, whereas the diamonds denote the second-order Raman modes of diamond. The inset shows the Raman lattice modes in the spectral region of 0−500 cm^{-1}.

TABLE 1: Observed Raman Shifts and IR Frequencies for α-$Ca(BH_4)_2$ at Near Ambient Pressure and Room Temperature with Assignments

Raman (cm^{-1})		IR (cm^{-1})			assignment	
this work[a]	reference[b]	this work[a]	reference[c]	reference[d]		
2412	2373/2382	2455	2415	2426	ν'_{3B}	asym B−H stretch
2356	2368/2376	2373	2356	2358	ν_{3A}	asym B−H stretch
2330	2311/2319	2332	2332	2332	ν_{3B}	asym B−H stretch
2274	2283/2285	2273[e]	2273	2271	ν_{1A}	sym B−H stretch
1367	1327	1337	1327	1330	ν_{2A}	in-plane BH_4^- bend
1237	1241	1239	1241	1244	ν'_{2A}	in-plane BH_4^- bend
1204	1204	1204	1204	1212	ν_{4B}	out-of-plane BH_4^- bend
1114	1117	1117	1117	1119	ν_{4A}	out-of-plane BH_4^- bend
1086	1089	1084	1089	1093	ν'_{4B}	out-of-plane BH_4^- bend
286	291					lattice mode
222	221					lattice mode

[a] Measured at room temperature and ambient pressure. [b] The frequencies for B−H stretching modes are from calculated values on D_{2h} site symmetry (see ref 14), whereas those for BH_4^- deformation are based on experimentally observed values (see ref 9). [c] Reference 9. Measured at 300 K. [d] Reference 9. Measured at 80 K. [e] Measured at 1.4 GPa.

splitting and a correlation field effect. However, the correlation field effect does not provide a measurable splitting for internal vibrations of BH_4^- at ambient pressure.[9,23,24] Therefore, we assign these modes based on static field splitting from an original T_d symmetry (A +E + 2T$_2$), which would result in nine both IR- and Raman-active modes (5A + 4B). The assignments for the observed Raman and IR modes based on the above principle are labeled in Figure 2 and listed in Table 1. In particular, the labels for these modes can be best understood with respect to the nature of molecular vibrations by following the convention of the original T_d symmetry in the format of ν_{iX}, where i = 1−4 corresponds to the modes in T_d symmetry [i.e., ν_1(A), ν_2(E), ν_3(T$_2$), and ν_4(T$_2$)], whereas X = A or B denotes their final site symmetries in the unit cell. Here, ν' or ν''denotes an otherwise degenerate mode (in T_d symmetry setting) that has the same vibrational origin (i) and site symmetry (A or B) as the corresponding ν mode. The designation of ν, ν', and ν'' is arbitrary.

For the IR spectrum of α-$Ca(BH_4)_2$ (Figure 2, spectrum a), the absorption bands in the 1000−1450 cm^{-1} region can be assigned as the deformation modes of the BH_4^- ion. In the region of 2000−2400 cm^{-1}, the strongest absorption band with a broad profile at 2332 cm^{-1} can be assigned as an asymmetric B−H stretching (ν_{3B}), with two weak shoulder bands at 2373 cm^{-1} (ν_{3A}) and 2455 cm^{-1} (ν'_{3B}) both associated with asymmetric B−H stretching. Besides the fundamental IR bands, additional bands were also observed as a result of the overtones and/or combinations of these fundamentals, which are labeled with asterisks in Figure 2. For instance, the band observed at 2159 cm^{-1} is very close to the overtone of ν'_{4B} (1084 cm^{-1}). Similarly, the bands at 2520 and 2450 cm^{-1} are likely to be the combinations involving ν_{2A} (1337 cm^{-1}), ν'_{2A} (1239 cm^{-1}), and ν_{4B} (1204 cm^{-1}) modes as $\nu_{2A} + \nu_{4B}$ and $\nu'_{2A} + \nu_{4B}$, respectively.

Although normal-mode analysis predicts that all internal modes of α-$Ca(BH_4)_2$ are both IR- and Raman-active, their band intensities are significantly contrasting (Figure 2) and their absolute frequencies also differ by a certain extent (Table 1). For example, only one broad-band profile associated with asymmetric B−H stretching was observed in the IR spectrum, whereas a well-resolved triplet (ν_{3B}, ν_{3A}, and ν'_{3B}) near 2350 cm^{-1} for this mode was observed in the Raman measurement. In addition, the symmetric B−H stretching mode ν_{1A}, which could not be observed in the IR spectrum, appeared as the most intense peak at 2274 cm^{-1} in the Raman spectrum. In the region of 1000−1450 cm^{-1}, all BH_4^- deformation modes were observed at similar frequencies as in the IR measurements, except for ν_{2A}, which has a markedly higher frequency than the corresponding IR and reference Raman frequency. Therefore, the assignment of this Raman mode is tentative. The inset of Figure 2 shows that two more Raman bands were observed at 286 and 222 cm^{-1}, which can be assigned as lattice modes (labeled as L$_2$ and L$_1$). The lattice profile is consistent with that reported by Fichtner et al.[9]

B. Raman Spectra on Compression. Starting from the ambient pressure, Raman spectra of $Ca(BH_4)_2$ were collected upon compression to 10.4 GPa and selected spectra are depicted in Figure 3. On the basis of the nature of vibrations, the Raman spectra are characterized in three regions, that is, the lattice region, the BH_4^- deformation region, and the B−H stretching region.

In general, all of the lattice modes shifted to higher frequencies with increasing pressure. In addition, more lattice modes evolved sequentially upon compression. For instance, a new lattice mode (labeled as L$_3$) appeared at 194 cm^{-1} at 2.3 GPa, suggesting a possible phase transition. Upon further compression to 3.9 GPa, another two new lattice modes at 284 and 309 cm^{-1} (labeled as L$_4$ and L$_5$, respectively) were observed, indicating another transformation in the crystal structure of $Ca(BH_4)_2$. Above 5.4 GPa, L$_4$ was significantly developed and became the

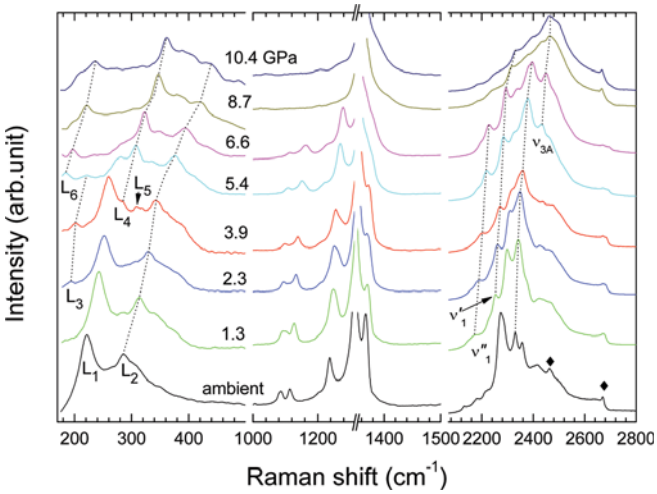

Figure 3. Selected Raman spectra of $Ca(BH_4)_2$ collected at room temperature on compression in the spectral regions of 180−500, 1000−1500, and 2100−2800 cm^{-1}. The relative intensities are normalized and thus are directly comparable. The assignments are labeled for selected Raman modes (see Figure 2). The dashed lines are for eye guidance to keep track of the pressure evolution of selected Raman bands.

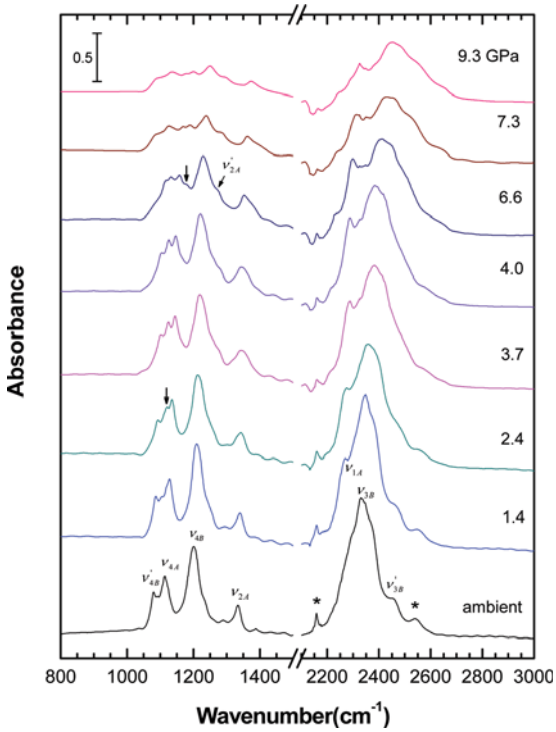

Figure 4. Selected IR spectra of $Ca(BH_4)_2$ collected at room temperature on compression in the spectral regions of 800−1500 and 2100−3000 cm^{-1}. The vertical bar labels the scale of the absolute absorbance intensity. The assignments are labeled for selected IR modes (see Figure 2). The vertical arrows denote the new modes observed during compression.

most intense lattice mode. Concurrently, a new lattice mode at 296 cm^{-1} (labeled as L_6) was also observed.

In the spectral region for BH_4^- deformation, four (ν_{2A}, ν'_{2A}, ν_{4A}, and ν'_{4B}) out of five predicted modes observed at 1367, 1237, 1114, and 1086 cm^{-1} all shift to higher frequencies with decreasing intensities upon compression. Above 8.7 GPa, no Raman modes in the BH_4^- deformation region could be clearly identified. In the B−H stretching region, the dominant ν_{1A} mode at 2274 cm^{-1} at ambient pressure rapidly lost its intensity upon compression and became a weak shoulder of ν_{3B} above 2.3 GPa. In contrast, the ν_{3B} mode, which is a B−H asymmetric stretching mode at 2330 cm^{-1}, evolved as the most intense peak at 2.3 GPa. The most significant change at 1.3 GPa was the observation of a new peak at 2253 cm^{-1} (labeled as ν'_1). As pressure was further increased to 2.3 GPa, another peak at 2189 cm^{-1} (labeled as ν''_1) became prominent. An interesting observation was that different modes exhibited a dominant intensity in different pressure regions, that is, ν_{1A} (<1.3 GPa), ν_{3B} (2.3−6.6 GPa), and ν_{3A} (>8.7 GPa). At the highest pressure of the current study (i.e., 10.4 GPa), all peaks became extremely weak and broad with strong interference from the second-order Raman band of diamond.

C. IR Spectra on Compression. Mid-IR spectra of $Ca(BH_4)_2$ were collected on compression to 9.3 GPa. Selected spectra are shown in Figure 4 in the spectral regions of 800−1500 and 2100−3000 cm^{-1} corresponding to the BH_4^- deformation and the B−H stretching, respectively. Upon compression, the most significant change in the IR profile was that the ν_{1A} mode was resolved at 2262 cm^{-1} as a shoulder band of ν_{3B}. In addition, a new band around 1120 cm^{-1} appeared at 2.4 GPa (labeled with a vertical arrow), suggesting a solid-to-solid phase transition. This phase transition was further evidenced by the abrupt broadening of the ν_{3B} band around this pressure. As the pressure was increased to 6.6 GPa, two more bands were observed, one of which could be deconvoluted with a frequency close to the ν'_{2A} mode, indicating another possible phase transition. Further compression to 7.3 GPa resulted in a prominent reduction of the IR intensities but with possibly more bands emerging in the BH_4^- deformation region. Overall, all bands became significantly broadened as the pressure increased. For instance, at the highest pressure (i.e., 9.3 GPa), the bandwidth for the ν_{3B} mode increased to ~200 cm^{-1} as compared with ~120 cm^{-1} at ambient pressure.

D. Pressure Effects on Raman and IR Modes. The pressure dependence of representative Raman and IR modes of $Ca(BH_4)_2$ was examined by plotting the vibrational frequency as a function of pressure and is shown in Figure 5 in three spectral regions, that is, the lattice region, the BH_4^- deformation region, and the B−H stretching region. For sharp, well-resolved Raman and IR bands (e.g., at low pressures), single Gaussian functions were used to determine the peak maxima while multiple Gaussian functions with controlled parameters were employed to deconvolute the overlapped bands, achieving an uncertainty of ±1 cm^{-1}. The pressure coefficients were analyzed by least-square fitting of the experimental data (with an average correlation coefficient $R = 0.99$) and are reported in Table 2. Possible phase transitions could be further inferred if sharp changes in the pressure coefficients were to be observed.

In general, all of the Raman and IR modes exhibited pressure-induced blue shifts, consistent with that the bonds become stiffened upon compression. In the lattice region, all modes can be fitted using different linear functions in different pressure regions, except for the L_1 and L_2 modes, which can be best fitted with a quadratic function below 2.3 GPa. A phase transition around this pressure is evident from the significant change in the pressure dependence of these two modes and the appearance of the L_3 mode. Subsequent phase transitions can be inferred by the appearance of the L_4 and L_5 modes at ~3.9 GPa and the L_6 at ~6.6 GPa. In the internal mode region, similarly, the distinct changes in the pressure dependence as well as the appearance/disappearance of the major Raman and IR modes also indicate consistent phase boundaries. In general, the pressure coefficients are the largest in the region below 2.3

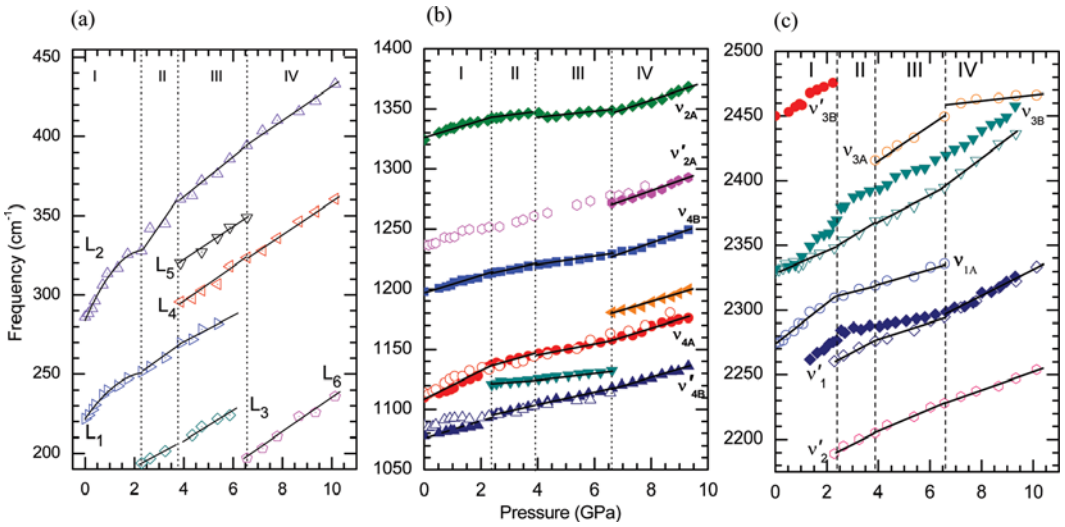

Figure 5. Pressure dependences of Raman and IR modes of $Ca(BH_4)_2$ on compression in (a) the lattice region (Raman only), (b) the BH_4^- deformation region, and (c) the B−H stretching region. Open and solid symbols denote respective Raman and IR modes. Different symbols denote Raman and IR modes with different origins. The solid lines crossing all symbols are based on linear regressions in different pressure regions, except for L_1 and L_2 modes in the pressure region of <2.3 GPa, which are fitted with quadratic functions. The vertical dashed lines indicate the proposed phase boundaries.

TABLE 2: Pressure Dependence of the Optical Modes of $Ca(BH_4)_2$ on Compression[a]

		dν/dP (cm^{-1}·GPa^{-1})			
optical mode	frequency[b] (cm^{-1})	phase I (<2.3 GPa)	phase II (2.3−3.9 GPa)	phase III (3.9−6.6 GPa)	phase IV (>6.6 GPa)
ν_{3A}	2356(2373)	8.9		13.6	2.2
ν_{3B}	2330(2332)	7.2 (20.1)	11.7 (15.6)	7.9 (9.7)	14.9 (14.4)
ν_{1A}	2274(2273)	16.9 (14.7)	5.0 (6.4)	6.1 (3.4)	20.4 (9.3)
ν'_1	2252	(15.7)	10.6 (2.5)	5.7 (4.0)	10.5 (10.1)
ν''_1	2187		9.9	8.5	7.1
ν_{2A}	1367(1337)	2.9 (7.2)	1.6 (2.7)	(2.7)	(9.9)
ν'_{2A}	1237(1241)	8.8	4.3	6.0	6.4 (8.4)
ν_{4B}	1204(1205)	(6.7)	(3.5)	(3.0)	(7.5)
ν_{4A}	1114(1117)	12.6 (12.3)	5.6 (5.9)	8.2 (4.4)	8.8 (7.1)
ν'_{4B}	1086(1084)	4.2 (6.5)	3.0 (5.7)	3.0 (4.7)	(6.4)
L_2	286	23.1	16.6	13.9	9.6
L_5	309			11.0	11.0
L_4	284			11.0	11.5
L_1	222	14.9	9.5	8.5	
L_3	194		8.1	9.1	
L_6	196				10.9

[a] Values refer to Raman modes, whereas those in parentheses refer to IR modes. [b] All frequencies were measured at ambient pressure and room temperature, except for L_3−L_6 modes, which were first observed during compression (see text).

GPa and decrease progressively across the boundaries at ∼2.3 and ∼3.9 GPa. Beyond 6.6 GPa, however, most pressure coefficients (except for ν_{3A}) increased markedly. Different pressure dependences are indicative of the different compressibilities of the different phases. Overall, the pressure dependence of the major Raman and IR modes collectively indicate several distinct pressure regions in which $Ca(BH_4)_2$ could exist in different phases. These pressure regions are <2.3, 2.3−3.9, 3.9−6.6, and >6.6 GPa, which we label as phases I, II, III, and IV, respectively.

E. Decompression. To better understand the pressure-induced structural evolutions and the high-pressure stability of $Ca(BH_4)_2$, Raman and IR spectra were collected on decompression all the way down to near-ambient pressure as well. During decompression, we observed similar, but very gradual, back transformations in both the Raman and the IR spectra with slightly delayed transformation pressures, indicating some degree of hysteresis. Nonetheless, as can be seen in Figure 6, nearly all of the fundamental modes observed before compression at ambient pressure were recovered upon decompression at a similar near-ambient pressure, although the intensities of some bands experienced noticeable modifications. All of these observations suggest that the pressure-induced structural transformations of α-$Ca(BH_4)_2$ are reversible and that α-$Ca(BH_4)_2$ is chemically stable in the entire pressure region examined in this study.

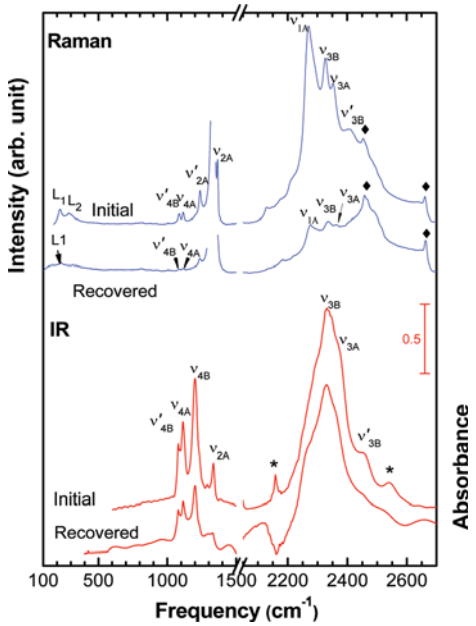

Figure 6. Raman (top panel) and IR (lower panel) spectra of recovered $Ca(BH_4)_2$ upon decompression as compared to their respective initial near ambient-pressure spectra before compression. The assignments are labeled for selected Raman and IR modes (see Figure 2). The Raman intensity is normalized with the arbitrary units labeled along the left vertical axis. The vertical bar along the right vertical axis indicates the absolute IR absorbance intensity.

F. Discussion. The ambient-pressure structure of $Ca(BH_4)_2$ has been extensively characterized by X-ray and neutron diffraction measurements as well as by computational approaches using density functional theory.[2,5,10,14] Although it is now well established that $Ca(BH_4)_2$ crystallizes into an orthorhombic structure at ambient pressure known as α phase, some

TABLE 3: Number of IR- and Raman-Active Modes for $Ca(BH_4)_2$ Observed at Pressures <2.3 GPa in Comparison with Predictions Using *Fddd* and *F2dd* Space Groups[a]

	observed		predicted			
			Fddd		*F2dd*	
spectral region	IR	Raman	IR	Raman	IR	Raman
lattice		2	12	15	20	27
bending	5	4	5 (10)	5 (10)	4 (8)	5 (10)
stretching	1−2	4	4 (8)	4 (8)	4 (8)	4 (8)

[a] The number in the parentheses for the internal modes refers to that with correlation field splitting.

controversy arises as to the detailed space group. The space group *Fddd* was originally proposed by several research groups.[9,14] Filinchuk et al.,[5] however, reported that a noncentrosymmetric space group *F2dd* is more favored than an *Fddd* crystal lattice based on the quantitative analysis of the diffraction pattern using the Rietveld method. It is, therefore, of interest to examine these two possibilities from a spectroscopic perspective. In addition to the normal-mode analysis for the BH_4^- internal vibrations described above, the irreducible representation of the lattice vibrations, including the translations of Ca^{2+} and BH_4^- as well as the BH_4^- rotations in the *Fddd* crystal lattice, is

$$\Gamma_{\text{lattice}}^{Fddd} = 2A_g + 5B_{1g} + 3B_{2g} + 5B_{3g} + 2A_u + 4B_{1u} + 2B_{2u} + 4B_{3u} \quad (4)$$

where all the gerade modes are Raman-active, whereas the ungerade modes are IR-active, except for the A_u mode, which is neither IR- nor Raman-active. As a result, if α-$Ca(BH_4)_2$ crystallizes into an *Fddd* space group, 15 Raman modes and 12 IR modes are expected in the lattice region. Apparently, both our Raman measurement where only two to six lattice modes were observed and that by Fichtner et al.,[9] who observed a total of four lattice modes at room temperature, suggest that only a subset of the lattice modes are detectable if the assumed crystal structure was correct.

In contrast, assuming *F2dd* (C_{2v}^{19}) as the space group for α-$Ca(BH_4)_2$ and by using the crystal data reported by Filinchuk[5] (i.e., Ca^{2+} on a C_2 site and BH_4^-on a general C_1 site), the irreducible representations for the BH_4^- internal vibrations and the lattice vibrations are

$$\Gamma_{BH_4^- \text{ vib}}^{F2dd} = (4A_1 + A_2 + 2B_1 + 2B_2) \times 2 \quad (5)$$

$$\Gamma_{\text{lattice}}^{F2dd} = 6A_1 + 7A_2 + 7B_1 + 7B_2 \quad (6)$$

where all species are Raman-active and species A_1, B_1, and B_2 are IR-active. As a result, a total of 18 internal and 27 lattice modes are Raman-active, whereas 16 internal and 20 lattice modes are IR-active. As mentioned above, because the correlation field splitting is unlikely to be observed with the current spectral resolution and/or very small intrinsic split magnitude, the number of observable internal modes would be halved, that is, nine Raman-active modes and eight IR-active modes.

In addition, on the basis of the nature of vibrations, two distinct spectral regions, that is, bending (1000−1400 cm^{-1}) and stretching (2200−2500 cm^{-1}), can be separated from the total irreducible representations. Table 3 summarizes the Raman- and IR-active modes in three spectral regions, that is, bending, stretching, and lattice regions under different space groups for comparison. As can be seen, the counting of the Raman bands in the lattice region does not allow for the unambiguous identification of the space group. In addition, we observed one to two IR-active modes and four Raman-active modes in the stretching region, which is consistent with both space groups. However, five IR-active modes and four Raman-active modes observed in the bending region point to a possible space group *Fddd*, whereas a total of only four IR modes were expected under the *F2dd* space group. Therefore, our measurements suggest that the crystal structure of $Ca(BH_4)_2$ in high-pressure (from ambient pressure to 2.3 GPa) phase I likely has a space group *Fddd*. To further confirm the identity of this centrosymmetric space group, measurements in the far-IR region would be helpful.

The crystal structure of another polymorph of $Ca(BH_4)_2$ produced at elevated temperatures, that is, the β phase, has also been studied using both experimental and theoretical approaches.[2,5] Although the space group for this phase was initially determined as $P4_2/m$,[10] Filinchuk et al.[5] and Majzoub et al.,[2] however, proposed that space group $P\bar{4}$ is more favored based on a careful Rietveld analysis. To our understanding, other than the extensive diffraction studies on α and β phases at ambient pressures, there has been no in situ X-ray or neutron data for $Ca(BH_4)_2$ that would allow for quantitative structural analyses at high pressures. However, three new high-pressure phases were identified in our spectroscopic study, making the β-phase structure a possible candidate for one of these high-pressure phases. This is particularly because higher-pressure phases are typically characterized by smaller unit cell volumes and thus by higher densities, whereas β-phase $Ca(BH_4)_2$ exhibits a density that is ∼3% higher than that for α phase. In addition, by using first-principles calculations, Majzoub et al.[2] examined the enthalpy as a function of the unit cell volume for several possible structures of $Ca(BH_4)_2$. It was predicted that, above 5.3 GPa, the preferred structure for $Ca(BH_4)_2$ has a tetragonal structure with space group $P\bar{4}$, the same as one of the proposed structures of β-$Ca(BH_4)_2$. In addition, the predicted transition pressure is in alignment with the pressure region of 3.3−6.7 GPa for which we claimed phase III. Therefore, it would be also of interest to examine the spectroscopic consistency in the context of these proposed space groups.

For the initially proposed space group for β-$Ca(BH_4)_2$, that is, $P4_2/m$ ($Z = 2$), Ca^{2+} occupies a C_{2h} site, whereas BH_4^- occupies a C_s site. Therefore, the irreducible representation for the internal modes and lattice modes are

$$\Gamma_{BH_4^- \text{ vib}}^{P4_2/m} = 3A_g + 3B_g + 2E_g + A_u + B_u + 3E_u \quad (7)$$

$$\Gamma_{\text{lattice}}^{P4_2/m} = 3A_g + 3B_g + 4E_g + 3A_u + 4B_u + 3E_u \quad (8)$$

where all gerade modes are Raman-active, whereas all the ungerade modes, except for the B_u modes, are IR-active. Therefore, a total of 8 Raman modes and 4 IR modes are expected for the BH_4^- vibrations and 10 Raman modes and 6 IR modes for the lattice vibrations. In contrast, for space group $P\bar{4}$ ($Z = 2$), where Ca^{2+} and BH_4^- occupy C_2 and C_1 sites, respectively, the irreducible representation for the internal and lattice modes are

$$\Gamma^{P\bar{4}}_{BH_4^- \text{ vib}} = (2A + 3B + 2E) \times 2 \quad (9)$$

$$\Gamma^{P\bar{4}}_{\text{lattice}} = 7A + 6B + 7E \quad (10)$$

where all species are Raman-active and species B and E are IR-active. As a result, a total of 14 (7 without correlation field splitting) internal and 20 lattice modes are Raman-active, whereas 10 (5 without correlation field splitting) internal and 13 lattice modes are IR-active. These analyses are summarized in Table 4. Apparently, the observation of a total of 8 Raman and 8 IR internal modes represent a closer match to those predicted assuming space group $P\bar{4}$ (i.e., 14 and 10, respectively). In contrast, the observed number of active Raman and IR internal modes does not match and, in most cases, exceeds the predicted number of modes in the individual bending and stretching regions under space group $P4_2/m$. Therefore, $P\bar{4}$ is more likely the structure for the high-pressure phase III from the spectroscopic perspective, if $Ca(BH_4)_2$ is to form a denser tetragonal phase. We further note that, if the assumption of space group $P\bar{4}$ is correct, then the correlation field splitting becomes significant to account for the total number of Raman- and IR-active modes, which is consistent with that the intermolecular interactions are markedly enhanced by compression.

The remaining questions concern the possible structures for phases II and IV. The phase between 2.3 and 3.9 GPa (labeled as phase II) could be regarded as an intermediate phase for the transition from phase I to phase III. This is evidenced by the fact that some modes that appear in either phase I or phase III, but not in both, coexist in phase II. The Raman and IR spectra above 6.6 GPa (phase IV) are characterized by significant band broadening and intensity reduction. At the highest pressure in this work (i.e., 10.4 GPa for Raman and 9.3 GPa for IR), all Raman modes and IR modes become extremely broad and weak, leaving significantly fewer distinguishable bands than before compression. The relatively sharp, well-resolved ruby fluorescence lines measured at different locations across the sample suggest that nonhydrostaticity or a pressure gradient that is typically responsible for the line broadening can be ruled out in this pressure region. All of these observations suggest that the structure of $Ca(BH_4)_2$ is becoming less ordered and may ultimately turn into an amorphous phase with further compression. Apparently, to understand the detailed structures of phases II and IV, in situ X-ray or neutron diffraction measurements are required with the aid of theoretical investigations.

We noticed that the pressure-induced phase transformations observed in our study were significantly different than those reported by George et al.[15] In their study, starting from a mixture of α- and β-$Ca(BH_4)_2$ at ambient pressure, no phase transitions were found for α-$Ca(BH_4)_2$ up to 13 GPa, as characterized by X-ray diffraction, whereas β-$Ca(BH_4)_2$ was found to undergo a structural transition to a highly disordered unknown structure above 10.2 GPa. The authors further claimed that α-phase $Ca(BH_4)_2$ was stable throughout the entire compression/decompression processes (i.e., no α-to-β transition was observed as predicted), whereas the transformation of β-$Ca(BH_4)_2$ was irreversible. Although the pressure reversibility of α-$Ca(BH_4)_2$ and its transformation into a disordered phase at high pressure for β-$Ca(BH_4)_2$ observed by George et al. are in close agreement with the results of our study, the detailed pressure effects on α-$Ca(BH_4)_2$ are highly contrasting between the two studies. This significant difference is likely associated with the fact that the starting materials had different compositions; for example, George et al.[15] started with a mixture of α- and β-$Ca(BH_4)_2$, whereas we used pure α-$Ca(BH_4)_2$. Although those authors did not specify the ratio between these two phases in the starting materials, their ambient-pressure Rietveld refinement clearly suggests that almost an equal amount of the two phases coexists even from the very beginning, thus increasing the possibility of the interactions/complexations between these two phases upon compression. Moreover, the authors acknowledged that a partial decomposition of the sample, leading to the release of molecular hydrogen, was observed around 2.5 GPa, which further complicates the sole pressure effects and their subsequent analysis. Apparently, in situ high-pressure X-ray diffraction measurements on pure phases of $Ca(BH_4)_2$ are needed to elucidate the exact details of the pressure-induced transformations.

TABLE 4: Number of IR- and Raman-Active Modes for $Ca(BH_4)_2$ Observed at 3.9−6.6 GPa in Comparison with Predictions Using $P4_2/m$ and $P\bar{4}$ Space Groups[a]

	observed		predicted			
			$P4_2/m$		$P\bar{4}$	
spectral region	IR	Raman	IR	Raman	IR	Raman
lattice		5	6	10	13	20
bending	5	4	3	2	3 (6)	4 (8)
stretching	3	4	1	6	2 (4)	3 (6)

[a] The number in the parentheses for the internal modes refers to that with correlation field splitting.

Conclusions

In this study, the effects of pressure on the structures of $Ca(BH_4)_2$ were investigated by Raman and IR spectroscopies up to ~10 GPa. Upon compression, three phase transitions were observed at near 2.3, 3.9, and 6.6 GPa, as evidenced by changes in the peak profiles and the pressure dependence of the characteristic Raman and IR modes over different pressure ranges. Spectroscopic measurements on decompression suggest that these pressure-induced transitions are reversible with the chemical structure of $Ca(BH_4)_2$ intact, indicating that $Ca(BH_4)_2$ is stable up to the pressure levels achieved in this study. Spectral analyses based on our combined Raman and IR measurements suggest that the high-pressure phase I exists between the ambient pressure and ~2.3 GPa while maintaining the known α-phase structure with space group *Fddd*. In the pressure region of 3.7−6.6 GPa, $Ca(BH_4)_2$ may exist as a denser tetragonal phase, consistent with previous first-principles calculations. Our detailed factor group analysis suggests that, in the structure of phase III, $Ca(BH_4)_2$ is more likely to be $P\bar{4}$ rather than $P4_2/m$. The structures of phases II and IV require further experimental and theoretical investigations.

Acknowledgment. The authors acknowledge funding support from a Discovery Grant, a Research Tools and Instruments Grant from the Natural Science and Engineering Research Council of Canada, a Leaders Opportunity Fund from the Canadian Foundation for Innovation, and an Early Researcher Award from the Ontario Ministry of Research and Innovation.

References and Notes

(1) Wang, L. L.; Graham, D. D.; Robertson, I. M.; Johnson, D. D. *J. Phys. Chem. C* **2009**, *113*, 20088.
(2) Majzoub, E. H.; Ronnebro, E. *J. Phys. Chem. C* **2009**, *113*, 3352.
(3) Lee, Y. S.; Kim, Y.; Cho, Y. W.; Shapiro, D.; Wolverton, C.; Ozolins, V. *Phys. Rev. B* **2009**, *79*, 104107.
(4) Kim, Y.; Reed, D.; Lee, Y. S.; Lee, J. Y.; Shim, J. H.; Book, D.; Cho, Y. W. *J. Phys. Chem. C* **2009**, *113*, 5865.

(5) Filinchuk, Y.; Ronnebro, E.; Chandra, D. *Acta Mater.* **2009**, *57*, 732.

(6) Buchter, F.; Lodziana, Z.; Remhof, A.; Friedrichs, O.; Borgschulte, A.; Mauron, P.; Zuttel, A.; Sheptyakov, D.; Palatinus, L.; Chlopek, K.; Fichtner, M.; Barkhordarian, G.; Bormann, R.; Hauback, B. C. *J. Phys. Chem. C* **2009**, *113*, 17223.

(7) Kim, J. H.; Jin, S. A.; Shim, J. H.; Cho, Y. W. *J. Alloys Compd.* **2008**, *461*, L20.

(8) Kim, J. H.; Jin, S. A.; Shim, J. H.; Cho, Y. W. *Scr. Mater.* **2008**, *58*, 481.

(9) Fichtner, M.; Chlopek, K.; Longhini, M.; Hagemann, H. *J. Phys. Chem. C* **2008**, *112*, 11575.

(10) Buchter, F.; Lodziana, Z.; Rernhof, A.; Friedrichs, O.; Borgschulte, A.; Mauron, P.; Zuttel, A.; Sheptyakov, D.; Barkhordarian, G.; Bormann, R.; Chlopek, K.; Fichtner, M.; Sorby, M.; Riktor, M.; Hauback, B.; Orimo, S. *J. Phys. Chem. B* **2008**, *112*, 8042.

(11) Barkhordarian, G.; Jensen, T. R.; Doppiu, S.; Bosenberg, U.; Borgschulte, A.; Gremaud, R.; Cerenius, Y.; Dornheim, M.; Klassen, T.; Bormann, R. *J. Phys. Chem. C* **2008**, *112*, 2743.

(12) Ronnebro, E.; Majzoub, E. H. *J. Phys. Chem. B* **2007**, *111*, 12045.

(13) Riktor, M. D.; Sorby, M. H.; Chlopek, K.; Fichtner, M.; Buchter, F.; Zuettel, A.; Hauback, B. C. *J. Mater. Chem.* **2007**, *17*, 4939.

(14) Miwa, K.; Aoki, M.; Noritake, T.; Ohba, N.; Nakamori, Y.; Towata, S.; Zuttel, A.; Orimo, S. *Phys. Rev. B* **2006**, *74*, 155122.

(15) George, L.; Drozd, V.; Saxena, S. K.; Bardaji, E. G.; Fichtner, M. *J. Phys. Chem. C* **2009**, *113*, 15087.

(16) Somayazulu, M. S.; Finger, L. W.; Hemley, R. J.; Mao, H. K. *Science* **1996**, *271*, 1400.

(17) Mao, W. L.; Mao, H. K.; Goncharov, A. F.; Struzhkin, V. V.; Guo, Q. Z.; Hu, J. Z.; Shu, J. F.; Hemley, R. J.; Somayazulu, M.; Zhao, Y. S. *Science* **2002**, *297*, 2247.

(18) Strobel, T. A.; Somayazulu, M.; Hemley, R. J. *Phys. Rev. Lett.* **2009**, *103*, 065701.

(19) Xie, S. T.; Song, Y.; Liu, Z. X. *Can. J. Chem.* **2009**, *87*, 1235.

(20) Lin, Y.; Mao, W. L.; Mao, H. K. *Proc. Natl. Acad. Sci. U.S.A.* **2009**, *106*, 8113.

(21) Mao, H. K.; Xu, J.; Bell, P. M. *J. Geophys. Res.* **1986**, *91*, 4673.

(22) Dong, Z.; Song, Y. *J. Phys. Chem. C* **2010**, *114*, 1782.

(23) Harvey, K. B.; Mcquaker, N. R. *Can. J. Chem.* **1971**, *49*, 3272.

(24) Hagemann, H.; Gomes, S.; Renaudin, G.; Yvon, K. *J. Alloys Compd.* **2004**, *363*, 126.

JP1009115